Energy & Environmental Science

RSC Publishing

PAPER

View Article Online
View Journal | View Issue

Enhanced charge extraction in organic solar cells through electron accumulation effects induced by metal nanoparticles†

Cite this: *Energy Environ. Sci.*, 2013, **6**, 3372

Feng-xian Xie,[a] Wallace C. H. Choy,*[a] Wei E. I. Sha,[a] Di Zhang,[a] Shaoqing Zhang,[b] Xinchen Li,[a] Chi-wah Leung[c] and Jianhui Hou[b]

Received 19th July 2013
Accepted 10th September 2013

DOI: 10.1039/c3ee42440e

www.rsc.org/ees

Metal nanoparticles (NPs) have been used to enhance the performance of thin-film devices such as organic photovoltaics. In this paper, we propose and demonstrate electron extraction enhancement induced by charge accumulation effects of metal NPs. The metal NPs (Au and Ag NPs) are embedded in a titanium oxide (TiO_2) layer, functioning as a highly efficient transport layer for improving the performances of inverted organic solar cells (OSCs), which leads to significantly increased photocurrent and power conversion efficiency reaching 8.20%. Importantly, our results show that the optical plasmonic effect of metal NPs (Au NPs and Ag NPs) in the electron transport layer is a minor factor in improving the OSCs' efficiency. Instead, the charge extraction enhancement under solar illumination can be explained by the transfer of UV-excited electrons from the TiO_2 electron transport layer to metal NPs and the enhanced accumulation of the electrons in metal NPs–TiO_2 composites. The electron accumulation reduces the work function of the electron transport composite layer after UV illumination. The redistribution of charges in the UV-irradiated metal NPs–TiO_2 system can assist the charge extraction in OSCs. Multiphysics study is also conducted to explain the effects of the charge accumulation on device performances (*i.e.* improving short-circuit current without degrading the open-circuit voltage). Consequently, by incorporation of metal NPs, our experimental and theoretical results show that the NPs–TiO_2 transport layer, in which case the effect of doping is different from the conventional doping effects in semiconductors, exhibits very good charge extraction and collection at the electrode for efficient organic optoelectronic devices.

Broader context

One of the essential aspects in designing efficient and stable organic optoelectronic devices such as organic light emitting diodes (OLEDs) and solar cells (OSCs) is the engineering of interface carrier transport layers between the active layer and electrodes. Among various materials available for interface layers, inorganic transition metal oxides can be used to form good transport layers for organic devices with their wide range of energy-aligning capabilities. In this paper, we introduced Au and Ag nanoparticle (NPs)–TiO_2 composites (NPs–TiO_2) functioning as a highly efficient electron transport layer. The charge accumulation effects in the composite materials can enhance the charge extraction in OSCs, which leads to significantly increased photocurrent and power conversion efficiency of 8.20%. Interestingly, the optical plasmonic effect of Au and Ag NPs is a minor factor in improving the OSCs' efficiency. The experimental and theoretical analysis show that the enhanced charge extraction under solar illumination is induced by the transfer of UV-excited electrons from the TiO_2 electron transport layer and accumulated by Au or Ag NPs.

Introduction

Along with the development of novel organic materials and new processing techniques, the engineering of charge transport layers has become an important topic for high performance organic solar cells (OSCs).[1–3] Inorganic transition metal oxides have newly emerged and are promising candidates for fulfilling

[a]*Department of Electrical and Electronic Engineering, The University of Hong Kong, Pokfulam Road, Hong Kong, China. E-mail: chchoy@eee.hku.hk*

[b]*Institute of Chemistry, Chinese Academy of Sciences, Beijing 100190, China*

[c]*Department of Applied Physics, The Hong Kong Polytechnic University, Hung Hom, Kowloon, Hong Kong, China*

† Electronic supplementary information (ESI) available: Additional information details about *J–V* characteristics and performance summary of inverted P3HT:$PC_{61}BM$ OSCs using TiO_2 layers of different thickness as ETLs under solar illumination (AM1.5G), *J–V* characteristics of inverted P3HT:$PC_{61}BM$ OSCs using TiO_2, Au NPs–TiO_2 and Ag NPs–TiO_2 (with Au NPs and Ag NPs of different concentrations) as ETLs under solar illumination (AM1.5G). Transmission electron microscopy (TEM) image of Au NPs, Ag NPs and TiO_2, scanning electron microscopy (SEM) of the NPs–TiO_2 composite film, absorption spectra of TiO_2 and NPs–TiO_2 solutions. Equivalent circuit model for OSC devices in impedance spectroscopy measurement and Nyquist plot of TiO_2 and NPs–TiO_2 film as ETL in inverted OSCs with and without UV excitation. See DOI: 10.1039/c3ee42440e

the role of efficient transport layers because of their wide range of energy-aligning capabilities.[4–6] Another attractive merit of transition metal oxides compared with other charge transport layers, such as poly(3,4-ethylenedioxythiophene) poly(styrenesulfonate) (PEDOT:PSS) and Ca, is their stability which greatly improves the lifetime of organic devices.[7] Generally, oxides such as MoO_3, V_2O_5, and WO_3 are employed as hole transport materials,[8–10] whereas ones such as TiO_2 and ZnO are commonly used for fabricating efficient electron transport layers (ETLs).[11,12] Inverted poly(3-hexylthiophene) (P3HT):[6,6]-phenyl C_{61} butyric acid methyl ester ($PC_{61}BM$)-based OSCs using ZnO ETL with high efficiencies of over 4% have been reported.[13] Alternatively, an ETL using TiO_2 nanocrystals doped with Cs_2CO_3 also results in efficient performance (PCE of 3.9%) for inverted single-junction OSCs.[14] Notably, ETL materials such as ZnO and TiO_2 are transparent in the visible spectrum but absorb UV light; thus the thickness of these ETLs is tunable without loss of absorption in the visible region.[15] Owing to this feature, it has been demonstrated that these materials can act as effective optical spacers in OSCs.[16,17]

Recently, various metal nanoparticles (NPs) have been incorporated into OSCs for making use of the plasmonic effects[18,19] to enhance the light absorption of OSCs with ultrathin-active-layer configuration. By incorporation of metal NPs into the active layer of single-unit OSCs[20–22] and the interconnecting layer of tandem OSCs,[23] the optical effects of plasmonic NPs on enhancing the light absorption and thereby the device efficiency have been reported. However, there are no clear studies to use the charge accumulation properties of metal NPs[24,25] (distinguished from plasmonic effects) to enhance the carrier extraction of metal oxide based carrier transport layers of OSCs for improving device performances.

In our work, we propose and demonstrate the enhancement of electron extraction properties of TiO_2 ETL and thus performances of OSCs by incorporation of metal NPs into the TiO_2 layer. Small size (about 15 nm) Ag and Au NPs are embedded in the ETL (TiO_2). Under UV illumination, a large number of carriers are generated in the TiO_2 layer. Importantly, our experimental results show that by introduction of Au and Ag NPs in the TiO_2 films, the UV-excited electrons are transferred from TiO_2 to metal NPs and the improved charge accumulation in the NPs–TiO_2 composite contributes to the improvement of electron extraction in OSCs. Meanwhile, our results also show that the Ag and Au NPs do not contribute to the optical absorption enhancement in OSCs even though plasmonic resonances existed in the metal NPs incorporated TiO_2 film. Theoretical work has also been conducted to describe the observed improvement. When the NPs–TiO_2 composite is introduced in OSCs as ETL, the photocurrent increases notably compared to that of the pristine TiO_2 film, and the power conversion efficiency of 8.20% in OSCs is reached.

Results and discussion

Device performances of OSCs with NPs–TiO_2 composites

Fig. 1 shows the device performance of inverted OSCs using the NPs–TiO_2 layer as an efficient ETL. The device structure of the OSCs is ITO/TiO_2 or Au–TiO_2 or Ag–TiO_2/polymer–fullerene blend/MoO_3/Ag, as shown in Fig. 2. Transmission electron microscopy (TEM) images of Au NPs (15 nm), Ag NPs (15 nm) and TiO_2 nanocrystals (4 nm) are shown in Fig. S1 in the ESI.† The absorption of TiO_2, Au–TiO_2 and Ag–TiO_2 solutions is shown in Fig. S2. The morphology of the NPs–TiO_2 layer (around 20 nm thick) and elemental analysis are shown in Fig. S3–S5†. Optimization of TiO_2 thickness is detailed in Fig. S6 and Table S1 of the ESI.† We find that for the TiO_2 ETL, the thickness of 20 nm offers the best device performance. We therefore use TiO_2 of 20 nm to study the charge accumulation effects of metal NPs. For the active layer, the robust material system of P3HT:$PC_{61}BM$ as well as the efficient low-bandgap material of PBDTTT-C-T:$PC_{71}BM$ are investigated. Optimization of the concentration of Au NPs and Ag NPs is detailed in Fig. S7 and S8 and Tables S2 and S3 of the ESI,† respectively.

When incorporating Au NPs into the TiO_2 layer, the OSCs show a notable increase in the short-circuit current density (J_{SC}) of inverted P3HT:$PC_{61}BM$ OSCs compared with those without Au NPs (from 9.03 mA cm^{-2} to 10.35 mA cm^{-2}), as well as an improved fill factor (FF) (from 62.9% to 65.1%). This yields an improved average PCE of P3HT:$PC_{61}BM$ OSCs from 3.64% to 4.26%. For the case of Ag NPs, similar results are obtained with the average PCE of P3HT:$PC_{61}BM$ OSCs increased from 3.64% to 4.01%. By using the low bandgap polymer donor PBDTTT-C-T in

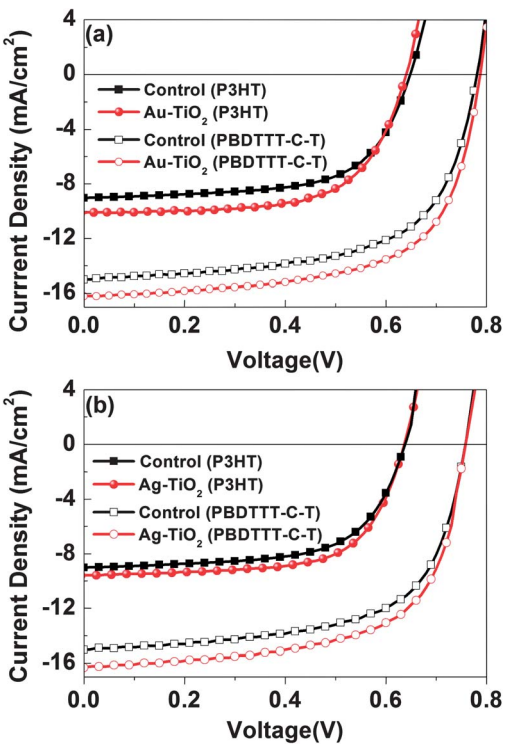

Fig. 1 (a) *J–V* characteristics of inverted P3HT:$PC_{61}BM$ OSCs and PBCTTT-C-T:$PC_{71}BM$ OSCs using TiO_2 and Au NPs–TiO_2 as ETLs under solar illumination (AM1.5G). (b) *J–V* characteristics of inverted P3HT:$PC_{61}BM$ OSCs and PBCTTT-C-T:$PC_{71}BM$ OSCs using TiO_2 and Ag NPs–TiO_2 as ETLs under solar illumination (AM1.5G).

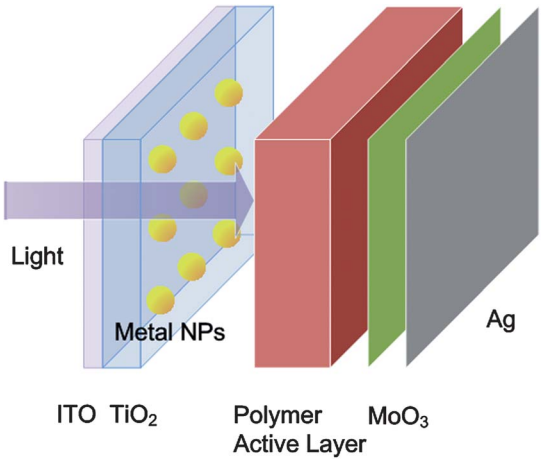

Fig. 2 Schematic of the inverted OSC device structure.

our inverted OSCs, the incorporation of Au NPs in the TiO_2 layer results in significantly enhanced device performance with J_{SC} increased from 15.02 mA cm^{-2} to 16.21 mA cm^{-2} and FF improved from 62.8% to 64.3%. The average PCE of PBDTTT-C-T:$PC_{71}BM$ is thus improved from 7.31% to 8.20%. Likewise, Ag NPs embedded in the TiO_2 layer result in enhanced device performance and the average PCE increased to 7.87%.

Effects of metal NPs in the TiO_2 layer on OSC performances

While one common contribution of plasmonic effects is the enhancement of absorption of OSCs, our results show that small metal NPs in TiO_2 will not enhance the absorption but the charge accumulation in the TiO_2 layer (as will be discussed later) and thus the PCE of OSCs. The absorption spectra of TiO_2/P3HT:PCBM and Au NPs–TiO_2/P3HT:PCBM are shown in Fig. 3(a), and for the case of Ag NPs, the absorption spectrum is shown in Fig. 3(b). We find no clear absorption changes in the active layer by incorporation of the Au or Ag NPs in TiO_2 even though plasmonic resonances existed in the metal NPs incorporated TiO_2 as shown in Fig. S2 in the ESI.† Consequently, optical enhancement of the metal NPs–TiO_2 OSCs is negligible. The reason for the small optical enhancement is that when light is incident normal into the device through ITO, the very strong field around metal NPs due to localized surface plasmon resonance (LSPR) mainly distributes laterally along the TiO_2 layer rather than vertically into the adjacent active layer.[26] Moreover, the NPs used in the experiment are relatively small (15 nm), thus the far field scattering effect is weak. Consequently, the metal NPs in the TiO_2 layer do not contribute to a clear absorption (optical) enhancement in OSCs.

The proposed UV-induced electron accumulation process by using the metal NPs is evidenced by blue shifts of the plasmonic absorption peaks after UV illumination, for both the Au and Ag NPs. The transmission spectra of Au and Ag NP-incorporated TiO_2 films before and after UV illumination are shown in Fig. 4. We find that the plasmonic absorption peak of Au NPs embedded in the TiO_2 film blue shifts from 560 nm (before UV illumination) to 552 nm (after UV illumination). Similarly, for the Ag NPs embedded TiO_2 film, the plasmonic peak blue shifts from 440 nm (before UV illumination) to 434 nm (after UV illumination).

Theoretically, the resonance frequency (ω) of localized plasmonic resonance (LPR) is described as

$$\omega = \frac{\omega_p}{\sqrt{1+2\varepsilon_d}} \quad (1)$$

where ω_p is the plasmon frequency of the metal and can be expressed as $\omega_p = [(ne^2)/(\varepsilon_o m)]^{1/2}$;[27] n and m are the electron density and effective mass of the electron of Au (or Ag) NPs

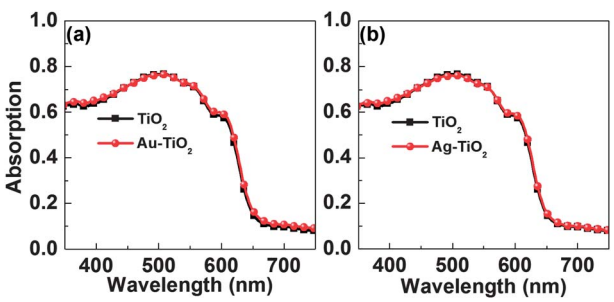

Fig. 3 (a) Absorption spectrum of the active layer (P3HT:$PC_{61}BM$) in inverted P3HT:$PC_{61}BM$ OSCs with TiO_2 and Au NPs–TiO_2 as ETLs. (b) Absorption spectrum of the active layer (P3HT:$PC_{61}BM$) in inverted P3HT:$PC_{61}BM$ OSCs with TiO_2 and Ag NPs–TiO_2 as ETLs.

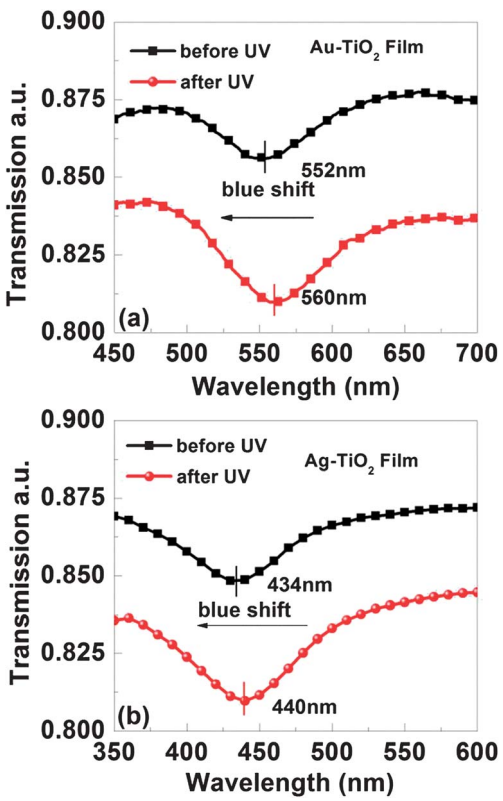

Fig. 4 (a) Transmission spectrum of the glass/ITO/Au–TiO_2 sample before and after UV illumination. (b) Transmission spectrum of the glass/ITO/Ag–TiO_2 sample before and after UV illumination.

respectively, e is the electron charge, and ε_d is the dielectric constant of TiO_2. Under UV illumination, a large number of electrons are generated in the TiO_2 layer. Different mechanisms in the NP-incorporated TiO_2 may result in the resonance frequency becoming smaller (red shift) or larger (blue shift). On one hand, under UV illumination, bounded electrons photoexcited from the valance band to the conduction band become free electrons, which will increase ε_d of TiO_2 (ref. 28 and 29) and thus reduce the resonance frequency ω. On the other hand, the increased free electrons in TiO_2 can transfer to the embedded metal NPs and n will increase. As a result, ω_p and thus the resonance frequency ω will increase. From the experimental results in Fig. 4, we observe a blue shift in the resonance peak wavelength after UV illumination for both the Au and Ag NP-incorporated TiO_2. The blue shift of the resonance peak confirms the electron accumulation by metal NPs and indicates that of the two processes discussed above, the transfer and accumulation of electrons from TiO_2 into metal NPs is the dominant process.

Besides the blue shift of the plasmonic peak confirming the charge accumulation as shown in Fig. 4, to further investigate and verify the electron accumulation in the metal NPs–TiO_2 composite, we conducted Kelvin probe measurement on TiO_2 films with and without Au and Ag NPs, which can intuitively characterize changes in the work function (WF) of UV-excited TiO_2 introduced by the metal NPs, and show the effects of the metal NPs in TiO_2 on the electron extraction of OSCs. Before starting the Kelvin probe measurement, all samples are put in a dark environment overnight to minimize the influence of light. All the samples are then illuminated under UV light (365 nm with 0.5 mW cm^{-2} intensity) for 15 min and then the WF of the samples is measured. A 15 min period is used for saturated illumination and stabilizing signals. After turning off the UV light, the samples are measured again continuously for 10 min. The sample WF is determined from the potential offset against a freshly cleaved highly ordered pyrolytic graphite sample with an assumed work function of 4.6 eV.[30]

The electron accumulation process by metal NPs in TiO_2 is corroborated by the temporal WF measurement of TiO_2 films in the dark after the UV light is turned off. Excited by the UV light, free electrons will be generated in TiO_2, increasing the carrier density.[31] However, after being cut off from saturated UV illumination, for TiO_2 samples without NPs, most of the photogenerated electrons will be lost to the electrodes or relax, corresponding to an increase of WF (or a downward shift of the Fermi level). As shown in Fig. 5, the WF increase of Au or Ag NP-embedded TiO_2 is distinctively different from that of NP-free TiO_2. The significantly lower WF of NP-embedded TiO_2 samples suggests a larger electron density, which accumulates under UV light and is retained by the metal NPs.

Furthermore, by comparison of the WF changes of TiO_2 samples prior to and after saturated UV illumination as shown in Fig. 6, it can be observed that UV illumination induces a much larger WF shift in the Au or Ag NPs–TiO_2 layers (thus a larger change in electron density), as well as a noticeably lower final WF than the pristine TiO_2 layer, despite the higher starting WF for the NPs–TiO_2 samples under the dark. For TiO_2 without any NPs, the change in WF, after UV illumination by 15 min, is rather small (0.21 eV), while for samples incorporated with Au or Ag NPs, the WF changes are clearly larger (0.32 eV for Au and 0.36 eV for Ag NPs), owing to the charge accumulation effects. Importantly, the final WF of both Au and Ag NP-embedded TiO_2 (4.35 and 4.36 eV, respectively) is noticeably smaller than that of TiO_2 without NPs (4.38 eV). Hence, a higher electron concentration in the TiO_2 layer under UV light is obtained by the introduction of the metal NPs in the TiO_2 layer. The increased carrier density in the NPs–TiO_2 layer by the electron accumulation can help reduce the contact resistance, which can facilitate the electron extraction in OSCs.

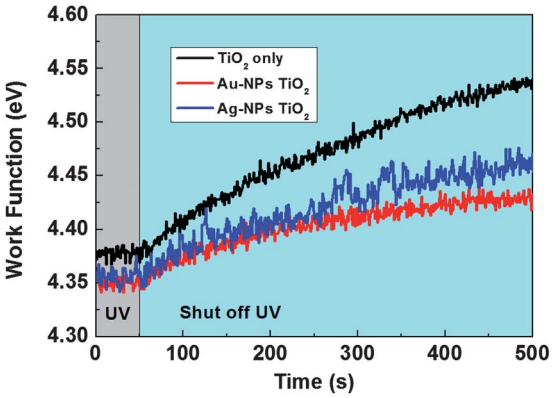

Fig. 5 Temporal WF changes of the TiO_2 film, Au NPs–TiO_2 film and Ag NPs–TiO_2 film measured by the Kelvin probe, after UV illumination for 15 min and the UV light is then turned off.

Indeed, by using impedance measurement, we characterize OSCs using TiO_2 ETL with or without metal NPs. We find that the extracted contact resistance is notably reduced for the NP-embedded device under UV light, as shown in Fig. S9 and Table S4 in the ESI.† It is very likely that the electron accumulation effects and thus the reduced contact resistance under UV light by incorporation of Au or Ag NPs in the TiO_2 ETL contribute to the enhanced performance in our OSCs. To further confirm the relationship between the enhanced device performance and the

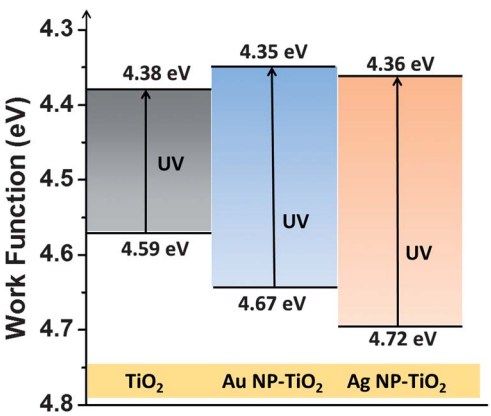

Fig. 6 Diagram of WF changes of the TiO_2 film, Au NPs–TiO_2 film and Ag NPs–TiO_2 film from the dark conditions to UV illumination (for 15 min), measured by the Kelvin probe.

electron accumulation process from the NPs–TiO_2 composite, we conducted theoretical studies of OSC devices with NPs–TiO_2 as ETLs, which revealed that the charge accumulation effects by the metal NPs were responsible for such performance enhancement in OSCs, as will be discussed later.

It is important to note that the effects of incorporating Au or Ag NPs in TiO_2 ETL are very different from conventional doping effects in semiconductors. Using Au NPs as an example, we investigate electron-only devices to study the electron transport and extraction properties of OSCs using NPs–TiO_2 ETL, as shown in Fig. 7. The structure of the electron-only device is ITO/TiO_2 or Au NPs–TiO_2 (20 nm)/P3HT:PC_{61}BM (220 nm)/Ca (20 nm)/Al (100 nm). A Ca/Al electrode is selected for electron collection and hole blocking purposes. When measured under the dark, the electron current density for the NPs–TiO_2 device is in fact lower than that of the NP-free device, suggesting that the mere presence of Au NPs without light excitation actually weakens the electron extraction in OSCs. This is distinctly different from the doping effects in semiconductors, where the dopant itself will enhance the electrical properties of the semiconductor. Interestingly, when the dark current of electron-only devices is measured after the device has been exposed to identical UV illumination, the electron current density of the NPs–TiO_2 device becomes notably larger, exceeding that of the NP-free device. The larger electron current density for NPs–TiO_2 suggests enhanced electron extraction under UV light, which is consistent with the improved OSC performance measured under simulated solar light (including UV light). Moreover, another important aspect supporting the difference between conventional doping and NP-induced effects in TiO_2 lies in the different shift of the Fermi level.

As shown in Fig. 6, the WF of the as-made TiO_2 samples under the dark measured using the Kelvin probe technique also supports the distinction between the charge accumulation effects and conventional doping. The WF of the as-made TiO_2 film actually increases after incorporating metal NPs (from 4.59 eV to 4.67 eV and 4.72 eV for Au and Ag NPs, respectively), possibly due to Schottky junction formation between the metal NPs and TiO_2.[28] The WF increase corresponds to a downward shift of the Fermi level, suggesting that unlike semiconductor doping, for the n-type TiO_2, embedding Au or Ag NPs in fact decreases its carrier concentration, which is initially detrimental to the electrical property. It is only after UV-induced charge accumulation that the WF and thus the electrical properties of the TiO_2 layer can be improved. Consequently, the effects introduced by incorporation of Au or Ag NPs into TiO_2 ETL should be distinguished from the doping effects in semiconductors.

Theoretical study of charge accumulation effects

We rigorously solve Maxwell's equations and organic semiconductor equations to study the electrical properties of OSCs, employing an electrical model integrated with our previously reported optical model of OSCs[32] for calculating the generation of excitons from light absorption in OSCs. The Poisson, drift-diffusion and continuity equations were solved self-consistently to produce *J–V* characteristics of OSCs. The details of the model are described in the theoretical model section.

The charge accumulation effects after introducing Au and Ag NPs are simulated by increasing the electron density (n) in the NPs–TiO_2 composite layer with a lower WF. As shown in Fig. 8, our theoretical results from the (optical and electrical) integrated device modeling show increased J_{SC} in OSCs with NPs–TiO_2 ETLs under simulated solar illumination, which agree well with our experimental results (see Table 1) with UV illumination. Compared with pristine TiO_2, the electron density (n) in the NPs–TiO_2 layer is higher due to the charge accumulation effects under UV illumination (which is confirmed from the wavelength shift of the plasmonic peak as shown in Fig. 4).

Since the electron drift current is given by $J_n = \sigma E = qn\mu_n E$, the higher charge density in the NPs–TiO_2 layer can increase the conductivity of the ETL, thus decreasing the CT resistance as observed in the impedance measurement. Furthermore, drift current through the NPs–TiO_2 ETL will be improved by the charge accumulation effects (with increased electron density n), which is dominant over diffusion current under short-circuit

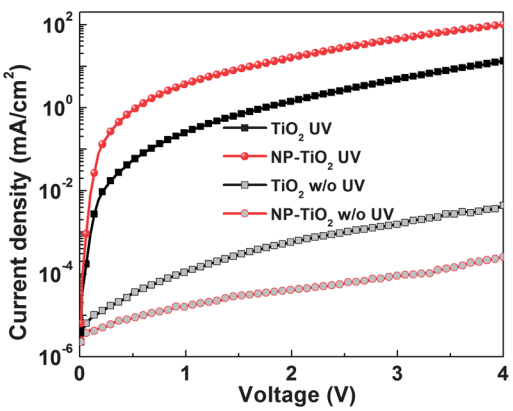

Fig. 7 *J–V* characteristics of electron-only devices using TiO_2 and optimized NPs–TiO_2 as ETLs measured with and without (w/o) UV excitation.

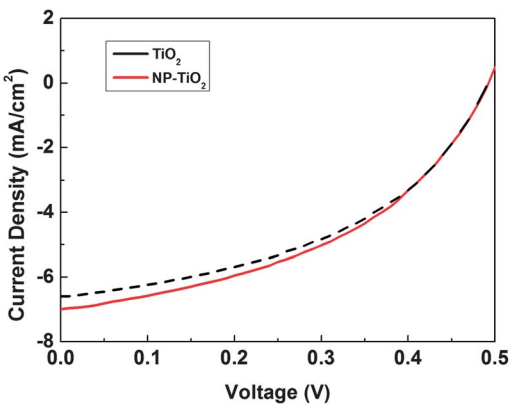

Fig. 8 Theoretical *J–V* characteristics of the OSCs with TiO_2 and NPs–TiO_2 as ETLs under simulated solar illumination. The charge accumulation effect after introducing Au and Ag NPs is simulated by increasing the electron density (n) in the TiO_2 layer.

Table 1 Device performance summary of inverted P3HT:$PC_{61}BM$ and PCBTTT-C-T:$PC_{71}BM$ OSCs with TiO_2, Au NPs–TiO_2 and Ag NPs–TiO_2 as ETLs under solar illumination (AM1.5G)

OSCs	V_{OC} (V)	J_{SC} (mA cm^{-2})	FF (%)	PCE (%)
TiO_2(P3HT)	0.640	9.03	62.9	3.64
Au–TiO_2(P3HT)	0.633	10.35	65.1	4.26
Ag–TiO_2(P3HT)	0.630	9.59	65.3	4.01
TiO_2(PBDTTT-C-T)	0.775	15.02	62.8	7.31
Au–TiO_2(PBDTTT-C-T)	0.787	16.21	64.3	8.20
Ag–TiO_2(PBDTTT-C-T)	0.760	16.32	63.44	7.87

conditions. Our experimental (Table 1) and theoretical (Fig. 8) results both show that the enhanced performance of OSCs is mainly from the increased short-circuit current in NPs–TiO_2 OSCs. Therefore, the introduction of Au and Ag NPs into TiO_2 mainly contributes to enhancing the drift current but not the diffusion current. Consequently, with our theoretical results, we show that after UV exposure, by incorporation of Au and Ag NPs into the activated TiO_2 layer, the short-circuit current and thus the device performance is significantly enhanced in the NPs–TiO_2 OSCs through the accumulation of charges in the NPs–TiO_2 composite.

Experimental section

Material synthesis and device fabrication

We choose to synthesize anatase phase TiO_2 nanocrystals and to stably mix them with Au and Ag NPs. The TiO_2 nanocrystals are synthesized by heating a mixture of titanium tetrachloride, ethanol and benzyl alcohol at 85 °C for 6 hours. The white precipitate is washed and redispersed in ethanol. Au NPs (15 nm in size) are synthesized by the reduction of $HAuCl_4$ by sodium citrate in water. Ag NPs (about 15 nm in size) are synthesized by the reduction of $AgNO_3$ by sodium tetrahydridoborate with PVP stabilization. For fabricating the Au or Ag NPs–TiO_2 films, a colloidal solution of Au NPs or Ag NPs with an average diameter of 15 nm mixed with TiO_2 anatase phase nanocrystals with 4 nm mean particle diameter (10 mg ml^{-1}) was prepared (as shown in Fig. S1 in the ESI†) to make a stable mixed solution. The mixed ratio of the two solutions (TiO_2 and NPs) is 2 : 1 and remains stable. The resulting solution was spin-coated on the indium tin oxide (ITO) substrate and annealed at 150 °C for 10 min, forming the NPs–TiO_2 layer (around 20 nm thick).

The scanning electron microscope (SEM) images and transmission electron microscopy (TEM) image of the NP-doped TiO_2 nanocomposite film can be found in Fig. S3 and S4†. The EDS element spectrum of the NPs-TiO_2 film is shown in Fig. S5†. All the TiO_2 layers (with or w/o NP doping) are ~20 nm thick which is optimized from the pristine TiO_2-based OSCs. Two polymer blends are employed as active layers to investigate device performances: one is a robust and well-known polymer blend of P3HT:[6,6]-phenyl-C_{61}-butyric acid methyl ester ($PC_{61}BM$), and the other is the newly synthesized poly{[4,8-bis-(2-ethyl-hexyl-thiophene-5-yl)-benzo[1,2-*b*:4,5-*b*′]dithiophene-2,6-diyl]-*alt*-[2-(2′-ethyl-hexanoyl)-thieno[3,4-*b*]thiophen-4,6-diyl]} (PBDTTT-C-T):$PC_{71}BM$. The inverted OSCs of glass/indium tin oxide (ITO)/TiO_2 or NPs–TiO_2 (~20 nm)/active layer (~220 nm for P3HT:$PC_{61}BM$, ~100 nm for PBDTTT-C-T):$PC_{71}BM$/MoO_3 (14 nm)/Ag (100 nm) are fabricated and studied.

Illuminated current density–voltage (*J*–*V*) characteristics were measured by using a Keithley 2635 source meter and an ABET AM1.5G solar simulator with a xenon arc lamp. The light source was calibrated using a NREL-calibrated Hamamatsu Si detector to produce solar illumination of AM1.5G.

Theoretical model

The electrical properties of OSCs can be modelled by solving semiconductor equations involving Poisson, drift-diffusion and continuity equations[33]

$$\nabla(\varepsilon\nabla\phi) = -q(p - n) \tag{2}$$

$$\frac{\partial n}{\partial t} = \frac{1}{q}\nabla(q\mu_n n\boldsymbol{E}_n + qD_n\nabla n) + QG - (1 - Q)R \tag{3}$$

$$\frac{\partial p}{\partial t} = -\frac{1}{q}\nabla\left(q\mu_p p\boldsymbol{E}_p - qD_p\nabla p\right) + QG - (1 - Q)R \tag{4}$$

where q is the electron charge, ϕ is the potential, and n and p are electron and hole concentrations. Moreover, μ_n and μ_p are the mobility of electrons and holes, which can be described by the field-dependent Frenkel–Poole form.[34,35] Furthermore, D_n and D_p are the diffusion coefficients accessible by the Einstein relations and mobility. $J_n = q\mu_n nE_n + qD_n\nabla n$ and $J_p = q\mu_p pE_p - qD_p\nabla p$ are respectively electron and hole current densities, and G is the exciton generation rate that is proportional to the incident light intensity. Here, the recombination rate R is taken as the Langevin bimolecular form,[35] and the field-dependent exciton dissociation probability Q is evaluated by the Onsager–Braun theory.[36,37] Several experimental studies[38] have found that the recombination rate in organic materials is smaller than the prediction of the Langevin theory $R = q(\mu_n + \mu_p)np/\varepsilon$, which was adopted in our theoretical model. As a result, our simulation result (Fig. 8) shows a lower fill factor than the experimental result (Fig. 1).

To take into account the carrier injection and extraction barrier due to the insertion of electron transport layer (ETL) such as TiO_2, the internal electric fields, which strongly affect the drift current, are given by

$$\begin{aligned} E_n &= -\nabla\varphi - \frac{\nabla\chi}{e} - \frac{k_B T}{e}\nabla\left[\ln(N_c)\right] \\ E_p &= -\nabla\varphi - \frac{\nabla\chi}{e} - \frac{\nabla E_g}{e} + \frac{k_B T}{e}\nabla\left[\ln(N_v)\right] \end{aligned} \tag{5}$$

where $\boldsymbol{E}_n$ and $\boldsymbol{E}_p$ are internal E-fields for electrons and holes respectively, χ is the electron affinity and E_g is the band gap, and N_c and N_v are effective density of states (DOS) for electrons and holes, respectively.

The boundary conditions play a key role in modelling electrical properties of OSCs. The potential boundary condition for the contact is given by

$$\phi = V_a - \frac{W_m}{q} \quad (6)$$

where V_a is the applied voltage, and W_m is the WF of the electrode. The charge accumulation effect after introducing metal NPs is simulated by injecting electrons in the NPs–TiO_2 composite transport layer. Mathematically, we can add an additional term of generation rate in eqn (3), which is non-zero only in the TiO_2 layer.

Conclusions

We propose and demonstrate enhanced charge density and charge extraction in TiO_2 as a highly efficient transport layer for improving the OSC performances by the incorporation of metal NPs. By using Au or Ag NP-incorporated TiO_2, PCE of inverted OSCs can reach 8.20% and 7.87%, respectively. The enhanced charge extraction in the NPs–TiO_2 composite can be attributed to the electron accumulation in the NPs–TiO_2 layer under UV illumination. The experimental and theoretical study show that the electron stored NPs–TiO_2 layer can lead to the reduction of the charge transport resistance and enhanced electron extraction. As a result, the photocurrent and thus the device performance of OSCs are increased considerably. Since TiO_2 can be used as ETL for organic light emitting diodes and OSCs, the work contributes to enabling efficient organic optoelectronic devices with practical applications.

Acknowledgements

This work is supported by University Grant Council of the University of Hong Kong (grants #10401466 and #201111159062), and the General Research Fund (grants: HKU#712010E and HKU711612E), the RGC-NSFC grant (N_HKU709/12) from the Research Grants Council of Hong Kong Special Administrative Region, China and the National Natural Science Foundation of China (no. 61201122). J. H. Hou thanks the financial support from National High Technology Research and Development Program 863 (2011AA050523). We acknowledge the help of Shumian Lu for proof-reading the manuscript.

Notes and references

1 H. L. Yip and A. K. Y. Jen, *Energy Environ. Sci.*, 2012, **5**, 5994–6011.
2 Z. He, C. Zhong, S. Su, M. Xu, H. Wu and Y. Cao, *Nat. Photonics*, 2012, **6**, 591–595.
3 B. J. Worfolk, T. C. Hauger, K. D. Harris, D. A. Rider, J. A. M. Fordyce, S. Beaupré, M. Leclerc and J. M. Buriak, *Adv. Energy Mater.*, 2012, **2**, 361–368.
4 M. T. Greiner, M. G. Helander, W.-M. Tang, Z.-B. Wang, J. Qiu and Z.-H. Lu, *Nat. Mater.*, 2012, **11**, 76–81.
5 J. Meyer, S. Hamwi, M. Kröger, W. Kowalsky, T. Riedl and A. Kahn, *Adv. Mater.*, 2012, **24**, 5408–5427.
6 V. Shrotriya, G. Li, Y. Yao, C. W. Chu and Y. Yang, *Appl. Phys. Lett.*, 2006, **88**, 073508.
7 M. Jørgensen, K. Norrman and F. C. Krebs, *Sol. Energy Mater. Sol. Cells*, 2008, **92**, 686–714.
8 F. Xie, W. C. H. Choy, C. Wang, X. Li, S. Zhang and J. Hou, *Adv. Mater.*, 2013, **25**, 2051–2055.
9 S. Han, W. S. Shin, M. Seo, D. Gupta, S.-J. Moon and S. Yoo, *Org. Electron.*, 2009, **10**, 791–797.
10 Y. Sun, C. J. Takacs, S. R. Cowan, J. H. Seo, X. Gong, A. Roy and A. J. Heeger, *Adv. Mater.*, 2011, **23**, 2226–2230.
11 C. C. Chen, L. Dou, R. Zhu, C. H. Chung, T. B. Song, Y. B. Zheng, S. Hawks, G. Li, P. S. Weiss and Y. Yang, *ACS Nano*, 2012, **6**, 7185–7190.
12 C. E. Small, S. Chen, J. Subbiah, C. M. Amb, S. W. Tsang, T.-H. Lai, J. R. Reynolds and F. So, *Nat. Photonics*, 2012, **6**, 115–120.
13 H. L. Yip, S. K. Hau, N. S. Baek, H. Ma and A. K. Y. Jen, *Adv. Mater.*, 2008, **20**, 2376–2382.
14 J. You, C. C. Chen, L. Dou, S. Murase, H. S. Duan, S. A. Hawks, T. Xu, H. J. Son, L. Yu, G. Li and Y. Yang, *Adv. Mater.*, 2012, **24**, 5267–5272.
15 R. Steim, F. R. Kogler and C. J. Brabec, *J. Mater. Chem.*, 2010, **20**, 2499–2512.
16 J. Y. Kim, S. H. Kim, H. H. Lee, K. Lee, W. Ma, X. Gong and A. J. Heeger, *Adv. Mater.*, 2006, **18**, 572–576.
17 A. K. K. Kyaw, D. H. Wang, D. Wynands, J. Zhang, T. Q. Nguyen, G. C. Bazan and A. J. Heeger, *Nano Lett.*, 2013, **13**, 3796–3801.
18 H. Chen, L. Shao, Q. Li and J. Wang, *Chem. Soc. Rev.*, 2013, **42**, 2679–2724.
19 L. Lu, Z. Luo, T. Xu and L. Yu, *Nano Lett.*, 2012, **13**, 59–64.
20 D. H. Wang, D. Y. Kim, K. W. Choi, J. H. Seo, S. H. Im, J. H. Park, O. O. Park and A. J. Heeger, *Angew. Chem.*, 2011, **123**, 5633–5637.
21 C. C. D. Wang, W. C. H. Choy, C. Duan, D. D. S. Fung, W. E. I. Sha, F. X. Xie, F. Huang and Y. Cao, *J. Mater. Chem.*, 2012, **22**, 1206–1211.
22 F. X. Xie, W. C. H. Choy, C. C. D. Wang, W. E. I. Sha and D. D. S. Fung, *Appl. Phys. Lett.*, 2011, **99**, 153304.
23 J. Yang, J. You, C. C. Chen, W. C. Hsu, H. R. Tan, X. W. Zhang, Z. Hong and Y. Yang, *ACS Nano*, 2011, **5**, 6210–6217.
24 A. Takai and P. V. Kamat, *ACS Nano*, 2011, **5**, 7369–7376.
25 M. Salvador, B. A. MacLeod, A. Hess, A. P. Kulkarni, K. Munechika, J. I. L. Chen and D. S. Ginger, *ACS Nano*, 2012, **6**, 10024–10032.
26 D. D. S. Fung, L. Qiao, W. C. H. Choy, C. Wang, W. E. I. Sha, F. Xie and S. He, *J. Mater. Chem.*, 2011, **21**, 16349–16356.
27 T. Hirakawa and P. V. Kamat, *J. Am. Chem. Soc.*, 2005, **127**, 3928–3934.
28 S. Mubeen, G. Hernandez-Sosa, D. Moses, J. Lee and M. Moskovits, *Nano Lett.*, 2011, **11**, 5548–5552.
29 V. Spagnol, H. Cachet, B. Baroux and E. Sutter, *J. Phys. Chem. C*, 2009, **113**, 3793–3799.
30 M. M. Beerbom, B. Lägel, A. J. Cascio, B. V. Doran and R. Schlaf, *J. Electron Spectrosc. Relat. Phenom.*, 2006, **152**, 12–17.

31 H. Schmidt, K. Zilberberg, S. Schmale, H. Flugge, T. Riedl and W. Kowalsky, *Appl. Phys. Lett.*, 2010, **96**, 243305.
32 W. E. I. Sha, W. C. H. Choy and W. C. Chew, *Opt. Express*, 2010, **18**, 5993–6007.
33 W. E. I. Sha, W. C. H. Choy and W. C. Chew, *Appl. Phys. Lett.*, 2012, **101**, 223302.
34 L. J. A. Koster, E. C. P. Smits, V. D. Mihailetchi and P. W. M. Blom, *Phys. Rev. B: Condens. Matter*, 2005, **72**, 085205.
35 P. Laugevin, *Ann. Chim. Phys.*, 1903, 433.
36 C. L. Braun, *J. Chem. Phys.*, 1984, **80**, 4157–4161.
37 L. Onsager, *Phys. Rev.*, 1938, **54**, 554–557.
38 Y. Min Nam, J. Huh and W. H. Jo, *Sol. Energy Mater. Sol. Cells*, 2011, **95**, 1095–1101.